journal

J. Am. Ceram. Soc., 76 [5] 1132–36 (1993)

Vibrational Spectroscopy of Aluminum Nitride

Laurie E. McNeil

Department of Physics and Astronomy, University of North Carolina at Chapel Hill, Chapel Hill, North Carolina 27599-3255

Marcos Grimsditch

Materials Science Division, Argonne National Laboratory, Argonne, Illinois 60439

Roger H. French*

Central Research and Development, E. I. du Pont de Nemours & Company, Inc., Wilmington, Delaware 19880

A complete description of the first-order Raman and Brillouin spectra of single-crystal aluminum nitride is provided. The frequency has been measured and the symmetry identified of each of the Raman-active zone-center optic modes, and the five independent elastic constants have been measured. The widths of the principal Raman modes increase with increasing oxygen content up to a critical value of approximately 1 at.%, after which they are constant. This behavior supports the hypothesis of a change in the nature of the oxygen defect at that concentration.

I. Introduction

ALUMINUM NITRIDE is an insulator (or wide-band-gap semiconductor) which is of considerable importance in electronics technology due to its high thermal conductivity, low thermal expansion, high strength, transparency, and piezoelectric properties. Its direct band gap of 6.2 eV makes it attractive for possible future applications in electroluminescent devices operating in the ultraviolet, and to this end measurements of the optical spectra have recently been made and compared to calculated electronic band structures.[1] Most of the present applications of AlN, such as in heat-sink substrates for electronic devices, depend upon the high thermal conductivity of the material. In single crystals of high purity this can reach 320 W/(m·K) at room temperature,[2] but for sintered polycrystals values of 70–170 W/(m·K) are more typical.

Since thermal conduction consists of the diffusion of phonons through the solid, a fundamental understanding of the thermal properties of a solid requires knowledge of the vibrational modes of the single crystal. A variety of techniques, including Raman and Brillouin scattering, infrared absorption, neutron scattering, and ultrasonics can be used to probe the vibrational spectrum. Although Raman and Brillouin scattering probe only long-wavelength modes, they have the advantage that much smaller crystals are required than for neutron or ultrasonic studies. To date the study of single-crystal AlN has been restricted by a dearth of suitable samples, and as a result the limited information presently available in the literature is not totally consistent. We present in this work a complete Raman and Brillouin scattering study of the long-wavelength vibrations of single-crystal AlN. We also compare the Raman modes in low- and high-thermal-conductivity samples to illustrate the connection between the vibrational spectra and the thermal properties of the material. Because Raman and Brillouin scattering are techniques which are not widely used in the ceramic community, we have chosen to be somewhat tutorial in our discussion of the techniques and the interpretation of the results.

II. Experimental Methods

The Raman scattering experiments described herein were performed at room temperature using 514.5-nm light from an Ar^+ laser. A double monochromator was used to analyze the scattered radiation with a resolution of 1 cm^{-1}. The light was detected with a cooled photomultiplier tube equipped with photon-counting electronics. The laser light was plane polarized, and where appropriate the scattered light was polarization analyzed using a polarizing filter. Only Stokes spectra were recorded.

The Brillouin scattering experiments were also performed at room temperature. The same laser wavelength was used, but in this case from a single-mode Ar^+ laser. A (5 + 4)-pass tandem Fabry-Pérot interferometer was used to analyze the light, which was detected with a cooled photomultiplier tube. Both Stokes and anti-Stokes spectra were recorded.

The single-crystal samples used in this study were taken from a crystal grown by a sublimation–recondensation technique[3] at 2250°C. The crystal was amber in color (due perhaps to nitrogen vacancies or to tungsten impurities from the crucible in which it was grown) and contained 343 ± 17 ppm by weight of oxygen. Its thermal conductivity was 275 W/(m·K) at room temperature. Platelet-shaped samples with faces oriented along high-symmetry directions were cut from this crystal and polished; the orientation was determined by Laue diffraction.

We also made Raman measurements of commercial sintered polycrystalline samples of different thermal conductivities (Toshiba America, Westboro, MA), and of a sintered polycrystal (North Carolina State University, Chapel Hill, NC).

III. Raman and Brillouin Scattering in Single-Crystal AlN

Both Raman and Brillouin scattering consist of the inelastic scattering of an incident photon with the creation or annihilation of a fundamental excitation of the condensed phase. Although the excitation can be of many forms, e.g., magnetic, in this work we are concerned solely with vibrational excitations (phonons). Raman and Brillouin scattering differ in that the former involves optic vibrations, in which the motions of the atoms in a single unit cell are largely out of phase, whereas the latter involves acoustic vibrations, in which the atoms in a

R. A. Condrate—contributing editor

Manuscript No. 195541. Received June 30, 1992; approved October 12, 1992.
Work at Argonne National Laboratory supported by the U.S. Department of Energy, BES–Materials Sciences, under Contract No. W-31-109-ENG-38.
*Member, American Ceramic Society.

unit cell move largely in phase. Raman scattering thus gives information about the interatomic force constants within a unit cell, and Brillouin scattering provides a determination of the bulk elastic constants of the material. In an anisotropic solid, such as a single crystal, an analysis of the allowed transitions for a particular scattering direction and polarization reveals the symmetry of the various vibrations. The small momentum of the incident and scattered photons compared to the size of the Brillouin zone means that, for a one-phonon process, the phonon involved in the scattering has wavevector $\mathbf{q} \approx 0$, i.e., only zone-center (long-wavelength) modes are observed. For a more complete discussion of the physics of Raman and Brillouin scattering, the reader is referred to the standard literature.[4]

(1) Raman Scattering

AlN crystallizes at atmospheric pressure in the wurtzite structure (space group C_{6v}^4–$P6_3mc$) with four atoms in the unit cell.[5] After modes of pure translation (zero-frequency modes) are removed, there remain for any value of $\mathbf{q}$ three acoustic and six optic normal modes. A group theory analysis[6] for the point group C_{6v} reveals that, of the six optic modes, there is one of A_1 (Γ_1) symmetry, one of E_1 (Γ_5) symmetry, and two each of E_2 (Γ_6) and B_1 (Γ_3) symmetries. The A_1, E_1, and E_2 modes are Raman active, the A_1 and E_1 modes are infrared active, and the B_1 modes are inactive. The A_1 and E_1 modes are polar modes; i.e., the interaction of the vibrations with the long-range Coulomb field leads to an energy difference between the vibration polarized parallel to the direction of propagation of the phonon (LO mode) and that polarized perpendicular to $\mathbf{q}$ (TO mode).

The requirement that the product of the excitation amplitude, susceptibility, and incident polarization must be invariant under the transformations of the symmetry group of the crystal leads to selection rules for excitation of the Raman-active modes, depending on the direction of propagation and the polarization of the incident and scattered radiation relative to the symmetry axes of the crystal. For a polycrystalline sample without preferred orientation, all modes are excited in any measurement, but, by using various scattering geometries with a single-crystal sample, it is possible to identify the symmetry of each of the modes observed in the Raman spectra. Figure 1 shows the full Raman spectrum of a sintered AlN polycrystal. In the specific case of AlN, the susceptibility matrices for the three Raman-active symmetries are given in Table I. The c-axis of the crystal is taken as the z direction, and the x and y directions are perpendicular to z and to one another.

The scattering matrix element is formed by taking the product of the susceptibility matrix $\boldsymbol{\chi}$ with the incident and scattered polarization vectors $\boldsymbol{\varepsilon}_I$ and $\boldsymbol{\varepsilon}_S$: $|\boldsymbol{\varepsilon}_S \cdot \boldsymbol{\chi} \cdot \boldsymbol{\varepsilon}_I|^2$. For a particular combination of $\boldsymbol{\varepsilon}_I$ and $\boldsymbol{\varepsilon}_S$, this is nonzero only for certain symmetries. For example, if both the incident and scattered photons are polarized along the z direction so that $\boldsymbol{\varepsilon}_I = (0, 0, \varepsilon_I^z)$ and $\boldsymbol{\varepsilon}_S = (0, 0, \varepsilon_S^z)$, the scattering matrix element for the A_1 mode is given by

$$|\boldsymbol{\varepsilon}_S \cdot \boldsymbol{\chi} \cdot \boldsymbol{\varepsilon}_I|^2 = \left| (0,0,\varepsilon_S^z) \cdot \begin{bmatrix} a & & \\ & a & \\ & & b \end{bmatrix} \cdot \begin{pmatrix} 0 \\ 0 \\ \varepsilon_I^z \end{pmatrix} \right|^2 = |b \varepsilon_S^z \varepsilon_I^z|^2 \qquad (1)$$

and the matrix elements for the E_1 and E_2 modes are zero. This corresponds to the spectrum shown in Fig. 2, which was recorded by using plane-polarized incident laser light with the polarization direction along z and selecting the z-polarized component of the scattered light. This scattering geometry is referred to as "$x(zz)\bar{x}$", where the symbols outside the parentheses refer to the direction of propagation of the incident and scattered light and those inside refer to the polarization directions. Since the scattering matrix element in this geometry is nonzero only for A_1 modes, the single peak at 614 cm^{-1} must have this symmetry. The identification of the E_1 and E_2 modes is conducted in a similar manner, as shown in Figs. 3 and 4.

Because the A_1 and E_1 modes are polar, the energies of the longitudinal (LO) and transverse (TO) vibrations are not the same, nor are they observable for all propagation directions. In particular, the A_1 LO and the E_1 TO modes are active for propagation of the phonon along the c-axis of the crystal, whereas the

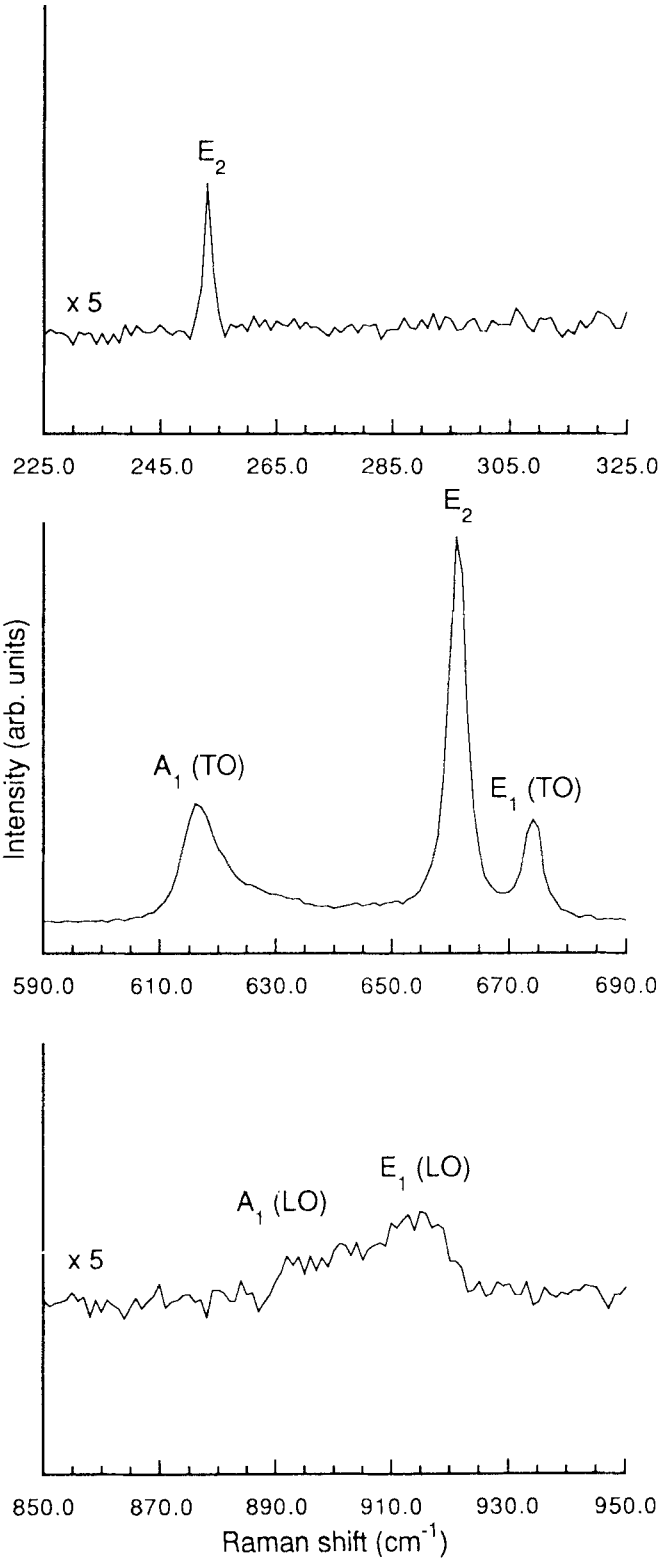

Fig. 1. Raman spectrum of commercial sintered polycrystalline AlN.

Table I. Susceptibility Matrices* χ for Raman-Active Modes of Point Group C_{6v}

A_1	E_1	E_2
$\begin{bmatrix} a & & \\ & a & \\ & & b \end{bmatrix}$	$\begin{bmatrix} & & c \\ & & \\ c & & \end{bmatrix}$ $\begin{bmatrix} & & \\ & & c \\ c & & \end{bmatrix}$	$\begin{bmatrix} d & & \\ & -d & \\ & & \end{bmatrix}$ $\begin{bmatrix} & -d & \\ -d & & \\ & & \end{bmatrix}$

*Reference 4, p. 327.

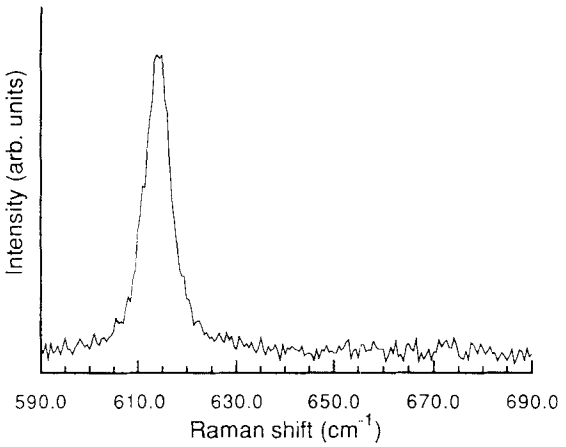

Fig. 2. Raman spectrum of single-crystal AlN in the $x(zz)\bar{x}$ scattering geometry (see text), in which only the A_1 mode is allowed.

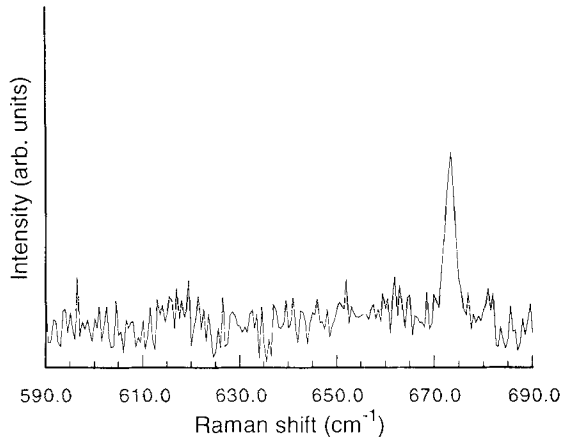

Fig. 3. Raman spectrum of single-crystal AlN in the $x(yz)\bar{x}$ scattering geometry (see text), in which only the E_1 mode is allowed.

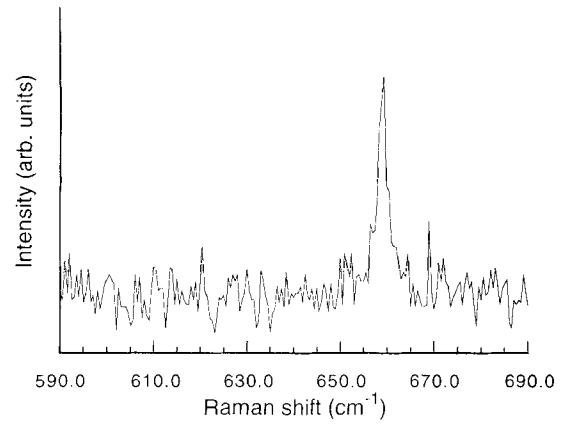

Fig. 4. Raman spectrum of single-crystal AlN in the $z(xy)\bar{z}$ scattering geometry (see text), in which only the E_2 mode is allowed.

A_1 TO and both of the E_1 modes are active for phonons propagating perpendicular to the c-axis. This provides additional confirmation of the symmetry identifications.

The end result of this analysis is the identification of all six peaks in the Raman spectrum. This identification is detailed in Table II. The frequencies are all measured with an error of ± 1.0 cm^{-1}.

Because suitable single crystals are seldom available, previous reports of Raman spectra in the literature have tended to disagree with one another, as shown in Table III. Brafman *et al.*[7] made measurements on whisker crystals which had their long axes in the c direction, which limited their choices of propagation directions. Tsu and Rutz[8] studied thin single crystals of platelet shape produced by evaporating sintered AlN in a H_2–N_2 forming gas at 1840°C. The faces of these crystals were not oriented in high-symmetry directions; therefore, their choice of propagation directions was also limited. Their measurements were made at 77 K. Sanjurjo *et al.*[9] considered the dependence of the Raman frequencies on pressure, using a thin film on a sapphire substrate. They did not report the crystallinity or orientation of the film, nor did they indicate how it had been produced. Carlone *et al.*[10] examined oriented polycrystalline films produced by sputtering onto silicon substrates. The orientation of the crystallites in the films varied across the sample, but largely restricted the propagation direction of the light to directions near the c-axis.

The disparities in frequency and symmetry assignment of the Raman modes listed in Table III can be attributed to the lack of

Table II. Raman Modes of AlN

Frequency (cm^{-1})	Symmetry
252	E_2
614	A_1 (TO)
660	E_2
673	E_1 (TO)
893	A_1 (LO)
916	E_1 (LO)

Table III. Previously Reported Raman Modes of AlN

Mode symmetry	Frequency (cm^{-1})	Reference
E_2	665	7
	303	10
	426	10
A_1 (TO)	667	7
	659	8
	659	9
E_1 (TO)	667	7
	672	8
	671	9
	614	10
A_1 (LO)	910	7
	897	8
	888	9
	663	10
E_1 (LO)	910	7
	912	8
	895	9
	821	10

high-quality single-crystal samples of the desired orientation used by previous workers. The measurements here reported do not suffer from the difficulties described in the cited reports: the spectra are intense and free of extraneous peaks, and the symmetry assignments of the modes can be made in an unambiguous manner with numerous checks for internal consistency.

(2) *Brillouin Scattering*

In a Brillouin scattering experiment, as in Raman scattering, we measure the frequency shift $\Delta\omega$ of the scattered photon. This is related to the sound velocity v in the crystal and to the acoustic phonon wavevector $\mathbf{q}$: $\Delta\omega = qv$. The sound velocity varies with direction in an anisotropic material such as a single crystal, and is different for longitudinal and transverse vibrations. The phonon wavevector is determined by the scattering geometry and by the wavevector $\mathbf{k}$ of the incident photon. Two geometries are relevant to the present work: *backscattering*, in which the photons enter and exit on the same face of the crystal and the phonon propagates roughly perpendicular to the crystal face, and *platelet*, in which incident and scattered photons enter and exit on opposite sides of a crystal with parallel surfaces, each at 45° to the crystal face. In the latter case the phonon propagates in the plane of the sample, and its direction in that plane can be varied relative to the crystal axes. For backscattering, the phonon wavevector is given by $q = 2nk$, where n, the effective index of refraction of the medium, is an appropriate combination of the ordinary and extraordinary indices as dictated by the polarization of the incident and scattered light. For the platelet geometry, $q = \sqrt{2}k$ and is independent of n.

The sound velocity in a particular crystal direction is related to the elastic constants of the crystal and to its density, ρ. For a crystal of hexagonal symmetry, such as AlN, there are five independent elastic constants: C_{11}, C_{33}, C_{44}, C_{12}, and C_{13}. These constants appear in various combinations in the solutions to the Christoffel equations for ρv^2 for different directions of propagation of the phonon.

For phonons propagating in the *bc*-plane of the crystal at an angle θ to the *c*-axis, the three solutions are a transverse wave with

$$\rho v^2 = \frac{1}{2}(C_{11} - C_{12}) \sin^2\theta + C_{44}\cos^2\theta \tag{2}$$

and quasi-longitudinal and quasi-transverse waves satisfying

$$\begin{aligned}\rho v^2 = {} & \frac{1}{2}(C_{11}\sin^2\theta + C_{33}\cos^2\theta + C_{44}) \\ & \pm \frac{1}{2}[(C_{11}\sin^2\theta + C_{33}\cos^2\theta + C_{44})^2 \\ & - 4C_{44}(C_{11}\sin^4\theta + C_{33}\cos^4\theta) \\ & + 4\sin^2\theta\cos^2\theta(C_{13}^2 + 2C_{13}C_{44} \\ & - C_{11}C_{33})]^{1/2}\end{aligned} \tag{3}$$

We have observed the latter two of these modes in the platelet geometry in a crystal which has the *c*-axis in the plane of the sample, and the values of ρv^2 are plotted in Fig. 5. The density $\rho = 3.255$ g/cm^3 has been used. For propagation along c ($\theta = 0°$) and b ($\theta = 90°$), we obtain C_{33} and C_{44} or C_{11} and C_{44} directly. C_{13} is then obtained by fitting the two solutions to Eq. (3) to the data, which gives the curves in Fig. 5. In the backscattering geometry from a sample with the *c*-axis perpendicular to the sample surface, we have been able to obtain an independent measurement of C_{33}.

For phonons propagating in the *ab*-plane, the three solutions to the Christoffel equations are independent of angle and yield $\rho v^2 = C_{11}$, $(C_{11} - C_{12})/2$, and C_{44}. For the sample with the *c*-axis perpendicular to the surface, we have observed the first two of these modes in the platelet geometry and have therefore been able to determine C_{12}. The values we obtain for all five elastic constants are shown in Table IV. In cases where we have had two independent data sets which involve the same constant

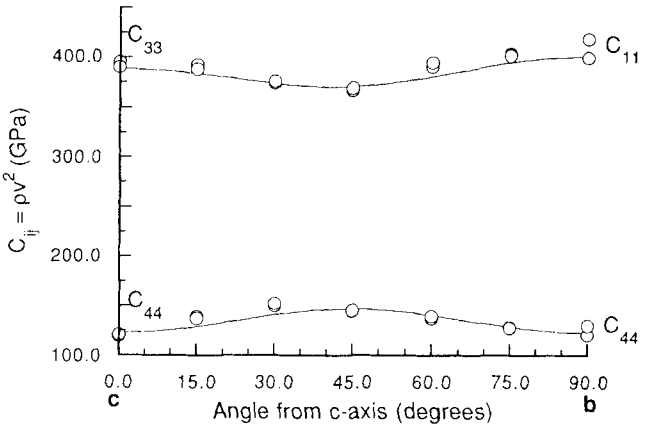

Fig. 5. Effective elastic constant $C_{ij} = \rho v^2$ for phonons propagating in the *bc*-plane, as a function of the angle between the *c*-axis and the propagation direction.

(C_{33}, C_{13}), the error limits are set by the best fits to the two data sets separately. In the other cases the uncertainties represent the variations in the measured values along high-symmetry directions.

Previous measurements of the elastic constants of AlN appear to be limited to a single surface acoustic wave (SAW) study by Tsubouchi *et al.*[11] in 1981. They used thin, single-crystal films with the *c*-axis perpendicular to the film surface grown by metalorganic chemical vapor deposition (MOCVD) on sapphire substrates. They were able to fit the variation as a function of frequency of the Rayleigh wave phase velocity and coupling coefficient by varying as fit parameters the five elastic constants, the two components of the permittivity, and the three components of the piezoelectric tensor. The data are rather scattered and the fitted curves do not describe the data particularly accurately, but the values obtained for the elastic constants compare well with our values obtained by the much more direct method of Brillouin scattering. Their measurements are included in Table IV.

These values show AlN to be a "hard" material, with elastic constants of the same order of magnitude as those of diamond. The average of the two compressional constants of AlN, $(C_{11} + C_{33})/2$, is 37% of the value of $C_{11} = 1076$ GPa in diamond,[12] and C_{44} is 22% of the 577 GPa observed in diamond. The shear mode C_{12} has a value of 125 GPa in diamond, almost identical to the average value $(C_{12} + C_{13})/2 = 124$ GPa in AlN. AlN is harder than the other wurtzite-structure nitrides GaN and InN,[13] with compressional constants approximately 40% larger than those of GaN and 120% larger than those of InN. The disparity in the shear constant C_{44} is even more remarkable, with reported values of 24 GPa in GaN and 10 GPa in InN compared to 125 GPa in AlN. The only constant reported to be larger in GaN and InN than in AlN is C_{13}, with values of 158 and 121 GPa compared to 98.9 GPa in AlN.

IV. Role of Oxygen

The high affinity of AlN for oxygen is well-known, and a variety of intermediate phases referred to as AlON exist[14] between pure AlN and pure Al_2O_3. Indeed, production of AlN

Table IV. Elastic Constants of AlN

Elastic constant	Value (GPa) This work	Ref. 11
C_{11}	410.5 ± 10.0	345
C_{33}	388.5 ± 10.0	395
C_{44}	124.6 ± 4.5	118
C_{12}	148.5 ± 10.0	125
C_{13}	98.9 ± 3.5	120

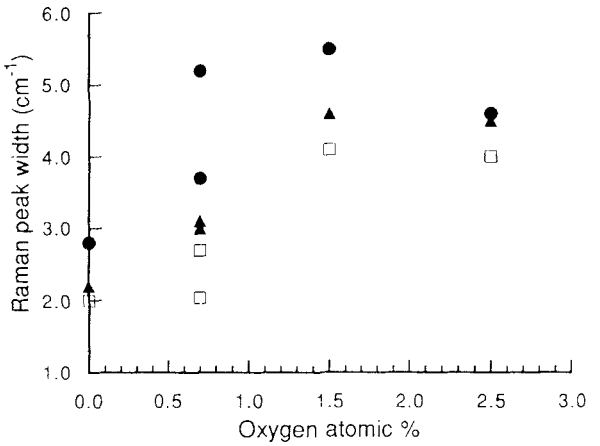

Fig. 6. Raman peak widths versus oxygen content for sintered polycrystalline AlN ((□) E_1 mode, (●) A_1 mode, and (▲) E_2 mode).

with oxygen content lower than 1 at.% is difficult, and typical sintered polycrystals contain several atomic percent oxygen. The presence of oxygen is associated with a reduction in the thermal conductivity of the material, which makes it less attractive for applications which benefit from a high thermal conductivity. It is therefore of interest to examine the coupling between the oxygen defect and the optic phonons in the crystal, which can be expected to contribute to phonon–phonon scattering at room temperature and above.

In recent years a variety of experiments performed on samples of varying oxygen content, including measurements of X-ray unit-cell volume, mid-gap luminescence, and thermal conductivity,[15] have pointed to the existence of a critical oxygen concentration of approximately 0.75 at.%. As the concentration of oxygen increases through that level, the change in the unit-cell volume shifts from contraction to expansion, the mid-gap luminescence ceases to red shift and begins to increase in intensity, and there is a break in the slope of the thermal conductivity. Taken together, these phenomena suggest that there is a change in the structure of the oxygen defect as the concentration increases above 0.75 at.%. The model that has been proposed by Harris, Youngman, and Teller[15] postulates that, at concentrations below 0.75 at.%, the oxygen substitutes for nitrogen in the lattice, with one aluminum vacancy occurring for every three substituted oxygen atoms. Above 0.75 at.% a new type of defect is stable, in which an aluminum atom is octahedrally bound to an increasing number of oxygen atoms. For each such defect formed, two aluminum vacancies are annihilated, which accounts for the expansion of the unit cell as the oxygen concentration is increased. This proposed change in the dominant defect would be expected to influence the normal modes of vibration which involve the defect site, and thus to affect the Raman spectrum.

The influence of oxygen on the Raman spectrum of AlN is shown in Fig. 6, where the widths of the three main peaks are plotted as a function of oxygen content in the sample. The width of a Raman peak increases with increasing structural disorder, which decreases the phonon lifetime. Here the widths show an increase in the neighborhood of 0.75 at.% oxygen and remain roughly constant at higher concentrations. This observation adds support to the hypothesis that the nature of the oxygen defect site changes as the oxygen concentration is increased, shifting from an isolated impurity to a more extended defect complex which would interact more strongly with the long-wavelength ($\mathbf{q} \approx 0$) first-order Raman modes.

A detailed examination of the interaction of the zone-center vibrations with the oxygen impurity requires a knowledge of the atomic motions associated with each normal-mode vibration. Such a calculation is in progress using a valence shell model.[16]

V. Summary

In this work we have provided a complete description of the first-order Raman and Brillouin spectra of single-crystal AlN. We have measured the frequency and identified the symmetry of each of the Raman-active, zone-center optic modes, and measured the five independent elastic constants. The widths of the principal Raman modes increase with increasing oxygen content up to a critical value of approximately 1 at.%, after which they are constant. This behavior supports the hypothesis of a change in the nature of the oxygen defect at that concentration.

Acknowledgments: We would like to thank Glen Slack of GE for providing us with the single crystal, and John Blum of Toshiba–Centronics and Robert Davis of North Carolina State University for providing polycrystalline samples. We would also like to thank Steven Loughin of GE for the sample preparation and characterization, and for helpful discussions.

References

[1]S. Loughin, "Vacuum Ultraviolet Spectroscopy and Analytical Critical Point Modeling of the Electronic Structure of Aluminum Nitride"; Ph.D. Dissertation. Department of Materials Science and Engineering, University of Pennsylvania, Philadelphia, PA, 1992.

[2]G. A. Slack, R. A. Tanzilli, R. O. Pohl, and J. W. Vandersande, "The Intrinsic Thermal Conductivity of AlN," *J. Phys. Chem. Solids*, **48** [7] 641–47 (1987).

[3]A. Slack and T. F. McNelly, "AlN Single Crystals," *J. Cryst. Growth*, **42**, 560–63 (1977).

[4]See, for example, W. Hayes and R. Loudon, *Scattering of Light by Crystals*. Wiley, New York, 1978; and, H. Poulet and J. P. Mathieu, *Vibration Spectra and Symmetry of Crystals*. Gordon and Breach, New York, 1976.

[5]H. Schultz and K. H. Themann, "Crystal Structure Refinement of AlN and GaN," *Solid State Commun.*, **23** [11] 815–19 (1977).

[6]See, for example, M. Tinkham, *Group Theory and Quantum Mechanics*. McGraw-Hill, New York, 1964.

[7]O. Brafman, G. Lengyel, S. S. Mitra, P. J. Gielisse, J. N. Plendl, and L. C. Mansur, "Raman Spectra of AlN, Cubic BN, and BP," *Solid State Commun.*, **6** [8] 523–26 (1968).

[8]R. Tsu and R. F. Rutz, "Raman Scattering in AlN Single Crystals"; pp. 393–95 in *Light Scattering in Solids*. Proceedings of Third International Conference (Campinas, Brazil, July 1975). Edited by M. Balkanski, R. C. C. Liete, and S. P. S. Porto. Flammarion, Paris, France, 1976.

[9]J. A. Sanjurjo, E. López-Cruz, P. Vogl, and M. Cardona, "Dependence on Volume of the Phonon Frequencies and the IR Effective Charges of Several III-V Semiconductors," *Phys. Rev. B: Condens. Matter*, **28** [8] 4579–84 (1983).

[10]C. Carlone, K. M. Lakin, and H. R. Shanks, "Optical Phonons of Aluminum Nitride," *J. Appl. Phys.*, **55** [11] 4010–14 (1984).

[11]K. Tsubouchi, K. Sugai, and N. Mikoshiba, "AlN Material Constants Evaluation and SAW Properties on AlN/Al_2O_3 and AlN/Si"; pp. 375–80 in *1981 Ultrasonics Symposium Proceedings* (Chicago, IL, Oct. 1981). Edited by B. R. McAvoy. IEEE, New York, 1981.

[12]M. H. Grimsditch and A. S. Ramdas, "Brillouin Scattering in Diamond," *Phys. Rev. B: Solid State*, **11** [8] 3139–48 (1975).

[13]M. E. Sherwin and T. J. Drummond, "Predicted Elastic Constants and Critical Layer Thicknesses for Cubic Phase AlN, GaN, and InN on β-SiC," *J. Appl. Phys.*, **69** [12] 8423–25 (1991).

[14]J. W. McCauley, K. M. Krishnan, R. S. Rai, G. Thomas, A. Zangvill, R. W. Doser, and N. D. Corbin, "Anion-Controlled Microstructures in the AlN–Al_2O_3 System"; pp. 577–600 in *Ceramic Microstructures '86*. Edited by J. A. Pask and A. G. Evans. Plenum Press, New York, 1987.

[15](a) J. H. Harris, R. A. Youngman, and R. G. Teller, "On the Nature of the Oxygen-Related Defect in Aluminum Nitride," *J. Mater. Res.*, **5** [8] 1763–73 (1990). (b) R. A. Youngman and J. H. Harris, "Luminescence Studies of Oxygen-Related Defects in Aluminum Nitride," *J. Am. Ceram. Soc.*, **73** [11] 3238–46 (1990).

[16]L. E. McNeil and K. S. Dy, in preparation (1993). □